

- The extracts were centrifuged at 100,000g for 15 min at 4°C. Immune complex kinase assays were done with extracts prepared from cells expressing epitope-tagged ERK2 (HA) or JNK1 (Flag). The epitope-tagged protein kinases were immunoprecipitated by incubation for 2 hours at 4°C with the M2 Flag monoclonal antibody (IBI-Kodak) or HA polyclonal antibody (BAbCo) bound to protein G-Sepharose (Pharmacia-LKB Biotechnology). The immunoprecipitates were washed twice with lysis buffer and twice with kinase buffer [25 mM Hepes (pH 7.4), 25 mM  $\beta$ -glycerophosphate, 25 mM  $MgCl_2$ , 0.5 mM DTT, 0.1 mM sodium orthovanadate]. The kinase assays were initiated by the addition of 1  $\mu$ g of substrate proteins (His6-Elk-1 or His6-SAP-1) (29) and 50  $\mu$ M [ $\gamma$ - $^{32}P$ ]ATP (10 Ci/mmol) in a final volume of 40  $\mu$ l. The reactions were terminated after 30 min at 25°C by the addition of Laemmli sample buffer. The phosphorylation of the substrate proteins was examined after SDS-PAGE by autoradiography. In-gel kinase assays were performed with 0.25 mg/ml of substrate protein (MBP, GST-ElkC, GST-SAPC, or GST-Jun) (29) polymerized in the gel as described (27). Phosphoamino acid analysis and phosphopeptide mapping of His6-Elk-1 phosphorylated by JNK1 was done as described (27). The horizontal dimension of the peptide maps was electrophoresis and the vertical dimension was chromatography.
29. Bacterial expression of GST-Jun was done as described (27). We constructed expression plasmids for GST-ElkC (Elk-1 residues 307 to 428) and GST-SAPC (SAP-1 residues 287 to 431) by subcloning PCR fragments of Elk-1 and SAP-1 in the Bam HI and Eco RI sites of pGEX-3X (Pharmacia-LKB Biotechnology). Glutathione-S-transferase (GST) fusion proteins were purified by glutathione affinity chromatography [D. B. Smith and K. S. Johnson, *Gene* 67, 31 (1988)]. The full-length Elk-1 protein (residues 1 to 428) fused to a COOH-terminal hexahistidine tag (His6-Elk-1) was expressed in bacteria with the plasmid pQE6/16Elk (8). The full-length SAP-1 protein (residues 1 to 431) fused to a COOH-terminal hexahistidine tag (His6-SAP-1) was expressed in bacteria with a plasmid constructed by the sequential ligation of three separate SAP-1 PCR fragments containing unique introduced restriction sites into the vector pET21d (Novagen). Hexahistidine fusion proteins were purified by nickel chelate affinity chromatography as described by the manufacturer (Novagen).
30. The DNA-binding activity of Elk-1 was examined by EMSA with  $^{32}P$ -labeled DNA probes. The E74 and SRE double-stranded oligonucleotide probes have been described (16). A 134-base pair (bp) PCR fragment of the *c-fos* promoter containing the SRE was prepared (5). Phosphorylation of His6-Elk-1 was done with recombinant ERK2 and JNK1 MAP kinases activated *in vitro* by the MAP kinase kinases MEK1 and MKK4, respectively. Epitope-tagged MKK4 was isolated from UV-irradiated transfected COS cells with the M2 monoclonal antibody (18). MEK1 was isolated from EGF-treated COS cells with the rabbit antibody 2880 [M. Wartmann and R. J. Davis, *J. Biol. Chem.* 269, 6695 (1994)]. Immune complex kinase assays were done with the MEK1 and MKK4 MAP kinase kinases and 6  $\mu$ g of bacterially expressed ERK2 and JNK1 (18) in kinase buffer (28) supplemented with 200  $\mu$ M ATP for 20 min at 22°C. The phosphorylated and activated MAP kinases (ERK2 and JNK1) were incubated with 0.5  $\mu$ g of His6-Elk-1 in 20  $\mu$ l of kinase buffer (28) supplemented with 100  $\mu$ M ATP for 20 min at 22°C. DNA-binding assays were done with 133 mM KCl and without salmon sperm DNA [A. D. Sharrocks, H. Gille, P. E. Shaw, *Mol. Cell. Biol.* 13, 123 (1993)] with 50 ng of Elk-1 for binding to the E74 probe and 10 ng of Elk-1 for ternary complex analysis at the SRE. Ternary complex formation assays were done with core<sup>SRE</sup> in the binding assays (7). Control experiments were done without ATP. Protein-DNA complexes were analyzed by PAGE (5% gel) in 1  $\times$  tris-borate EDTA and visualized by autoradiography.
31. SRE-dependent gene expression was monitored in cotransfection assays (25) with the reporter plasmid pSRE-Luc, which contains two copies of the *c-fos* SRE cloned upstream of a minimal promoter element and the firefly luciferase gene [A. Seth et

- al., *J. Biol. Chem.* 267, 24796 (1992)]. The activity of GAL4/ElkC (5) was measured in cotransfection assays with the reporter plasmid pG5E1bLuc [A. Seth et al., *J. Biol. Chem.* 267, 24796 (1992)]. This reporter plasmid contains five GAL4 sites cloned upstream of a minimal promoter element and the firefly luciferase gene. Transfection efficiency was monitored with a control plasmid that expresses  $\beta$ -galactosidase (pCH110; Pharmacia-LKB Biotechnology). The luciferase and  $\beta$ -galactosidase activity detected in cell extracts was measured [S. Gupta, A. Seth, R. J. Davis, *Proc. Natl. Acad. Sci. U.S.A.* 90, 3216 (1993)].
32. JNK activity was measured by an immune complex kinase assay with a rabbit polyclonal antibody to JNK

(14) and the substrate c-Jun. ERK activity was measured with the substrate MBP (22).

33. We thank N. Ahn, P. Shaw, R. Treisman, and M. Weber for providing reagents; B. Dérjard and I.-H. Wu for preparing the MKK4 vector; T. Barrett and R. Liddell for DNA sequence analysis; members of the Davis and Sharrocks laboratories for critical discussions; and M. Roberts for secretarial assistance. R.J.D. is an Investigator of the Howard Hughes Medical Institute. Supported by grants from the National Cancer Institute (R.J.D.), the North of England Cancer Research Campaign (A.D.S.), and the Royal Society (A.D.S.).

20 April 1995; accepted 23 June 1995

## Inactivation of the Mouse Huntington's Disease Gene Homolog *Hdh*

Mabel P. Duyao,\* Anna B. Auerbach,\*†, Angela Ryan,\*  
Francesca Persichetti, Glenn T. Barnes, Sandra M. McNeil,  
Pei Ge, Jean-Paul Vonsattel, James F. Gusella,  
Alexandra L. Joyner,† Marcy E. MacDonald‡

Huntington's disease (HD) is a dominant neurodegenerative disorder caused by expansion of a CAG repeat in the gene encoding huntingtin, a protein of unknown function. To distinguish between "loss of function" and "gain of function" models of HD, the murine *HD* homolog *Hdh* was inactivated by gene targeting. Mice heterozygous for *Hdh* inactivation were phenotypically normal, whereas homozygosity resulted in embryonic death. Homozygotes displayed abnormal gastrulation at embryonic day 7.5 and were resorbing by day 8.5. Thus, huntingtin is critical early in embryonic development, before the emergence of the nervous system. That *Hdh* inactivation does not mimic adult HD neuropathology suggests that the human disease involves a gain of function.

Huntington's disease is a dominant neurodegenerative disorder (1) with a characteristic pattern of neuronal loss (2) and consequent chorea, psychiatric alterations, and intellectual decline. HD results when one copy of the gene encoding huntingtin, an ~350 kD cytoplasmic protein found in fetal and adult peripheral tissues and nervous system (3–5), contains an expanded stretch of CAG trinucleotides. Although the CAG repeat is normally a Mendelian polymorphism (11 to 34 units), the HD expanded repeat (37 to more than 100 units) is unstable through meiotic transmission and its length is correlated with disease severity (3).

The HD defect probably acts at the protein level, as the HD CAG repeat is trans-

lated, altering huntingtin by elongating a polyglutamine segment near the NH<sub>2</sub>-terminus (4, 5). One possibility is that elongating the polyglutamine stretch reduces huntingtin's normal activity, but individuals with one copy of the normal gene inactivated by translocation do not develop HD despite a 50% reduction (6). However, a huntingtin loss of function could still cause HD if the abnormal protein also produces "dominant negative" inhibition of its normal counterpart. An alternative is that the polyglutamine segment confers a new property (gain of function) that may be unrelated to huntingtin's normal activity.

To choose between these models, we generated an inactivating mutation of the mouse *Hdh* gene (7) by targeted disruption. If HD involves a dominant loss of function, we would expect mice heterozygous for *Hdh* inactivation to be phenotypically normal (like their human counterparts with HD gene translocations) and mice homozygous for huntingtin inactivation to mature and manifest HD-like neuropathology. Alternatively, if HD involves a dominant gain of function, neither heterozygous nor homozygous inactivation of *Hdh* would produce HD-like neuropathology, but the latter might produce a completely different phenotype

M. P. Duyao, A. Ryan, F. Persichetti, G. T. Barnes, S. M. McNeil, J. F. Gusella, M. E. MacDonald, Molecular Neurogenetics Unit, Massachusetts General Hospital, Charlestown, MA 02129, USA.

A. B. Auerbach and A. L. Joyner, Division of Molecular and Developmental Biology, Mount Sinai Hospital, Toronto M5G1X5, Canada.

P. Ge and J. P. Vonsattel, Laboratory for Molecular Neuropathology, Massachusetts General Hospital, Charlestown, MA 02129, USA.

\*These authors contributed equally to this work.

†Present address: Developmental Genetics Program, Skirball Institute for Biomolecular Medicine, New York University Medical Center, New York, NY 10016, USA.

‡To whom correspondence should be addressed.

dictated by huntingtin's normal physiological role. To disrupt *Hdh* in embryonic stem (ES) cells, we used a vector that removes exons 4 and 5 and replaces them with the bacterial *neo* gene (Fig. 1A) (8). Five correctly targeted clones were identified (9), and two were used to isolate homozygous mutant cells in which the remaining normal allele was replaced by a second copy of the targeted insertion (10).

Protein immunoblots (5) confirmed that mouse huntingtin was expressed in both wild-type and heterozygous mutant ES cells (band intensity was reduced by about one-half) and that its expression was abolished in homozygous *Hdh* mutant ES cells (Fig. 1B). No truncated protein was produced from the mutant allele, as determined by careful examination of proteins in different size ranges (particularly 15 to 20 kD) with an NH<sub>2</sub>-terminal antiserum (5). This inactivating mutation was not a cell lethal, as homozygous cells were propagated for more than 1 month under standard culture conditions.

*Hdh* mutant mice (11) were produced from three independent heterozygous ES cell lines, and two lines were used for the bulk of the analysis. Heterozygous mice were indistinguishable from wild-type littermates in appearance, weight, movement, mating behavior, and response to handling. At age 4 months, eight heterozygotes and eight sex-matched wild-type littermates were examined by dissection with no evidence of phe-

notypic abnormality. Expression of only full-length huntingtin in the brain was confirmed in two heterozygotes (12). Blinded microscopic histological examination of the entire brain in serial sections ( $n = 6$ ) revealed no evidence of pathology or other diagnostic abnormality (12).

To assess the homozygous mutant phenotype, heterozygous *Hdh* mice were interbred, and at weaning mice were genotyped (Table 1). Of 236 progeny, about one-third were wild-type, about two-thirds were heterozygotes, and none were homozygotes. In addition, no homozygotes were detected at late embryonic stages [embryonic day (E) 18.5, E16.5, and E12.5]. At E9.5, five advanced resorption sites were found to represent homozygotes by genotyping of yolk sac DNA. At E8.5, nine resorbing embryos, consisting of a soft button of degenerating embryonic tissue and a small yolk sac, were all homozygotes (Table 1). Thus, inactivation of *Hdh* is an embryonic lethal and is not functionally analogous to the HD CAG expansion mutation in man.

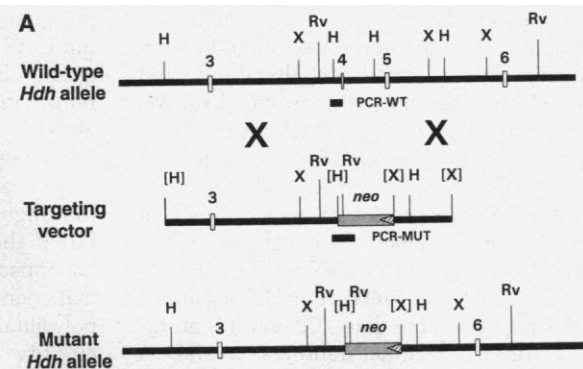
At E7.5, dissected embryos displayed two distinct morphological phenotypes (Fig. 2, A and B). Of 54 embryos genotyped (Table 1), approximately 42 displayed normal developmental features of this primitive streak stage and were either wild-type or heterozygous mutants. The remaining 12 were homozygotes and had a characteristic abnormal morphology. Although the yolk sac was of normal size, the embryo was about two-thirds

normal size and misshapen, with a prominent constriction between the extra-embryonic and embryonic regions. At E7.0, 14 normal embryos were either wild-types or mutant heterozygotes, whereas 6 abnormal embryos, distinctly smaller and thinner, were homozygotes (Table 1). Examination of three litters (30 implantations) of early to late egg-cylinder stage embryos (E6.5) did not reveal an obvious mutant phenotype.

In histologic sections at E7.5, the ectoplacental cone, parietal endoderm, and trophoblast giant cells of homozygotes appeared normal in shape and size. The extraembryonic region was reduced in size but grossly normal, possessing an amnion, chorion, and allantois (Fig. 2, C to D). The columnar cells of the extra-embryonic endoderm were not organized into a tight sheath but formed a folded layer that extended around the shrunken embryonic region.

The embryonic region of homozygotes was distinctly abnormal (Fig. 2, C to F). The primitive streak formed at one end, but no node structure was apparent. Mesoderm cells lined the yolk sac, amnion, and chorion, and surrounded the embryo adjacent to the primitive streak but did not extend to the distal pole. The embryonic ectoderm was symmetrical and featureless, without evidence of head folds. The cellular morphology of the ectoderm and mesoderm was abnormal, with the ectoderm thicker than normal and disorganized rather than columnar, especially distally, and abnormally rounded mesoderm cells densely, rather than loosely, packed. Although mitotic cells were present in all cell layers, ~10% of embryonic ectodermal cells exhibited pyknotic nuclei as compared with <1% in normal cells ( $n = 700$ ; seven adjacent sections). Preliminary whole-mount in situ hybridization at E7.5 revealed abnormal patterns of expression of early embryonic markers [*Brachyury* (*T*), *gsc*, and *HNF-3 $\beta$* ] (13). *Brachyury* (*T*) (Fig. 3) expression confirmed the morphological find-

**Fig. 1.** *Hdh* gene targeting. (A) Schematic diagram of targeting strategy. Physical map (~14 kb) shows *Hdh* exons 3 to 6 (open boxes) relative to Xba I (X), Hind III (H), and Eco RV (Rv) restriction sites. Square brackets denote sites eliminated in vector (pPNT-Hdh4/5) construction. PGK promoter and orientation within the *neo* cassette (stippled box) are denoted by arrow head. The Hsv-tk cassette is not shown. Homologous recombination (denoted by X) replaces exons 4 and 5 with *neo*. Elimination of *neo* by splicing would join exons 3 and 6



and introduce a frame shift truncating the protein 30 novel amino acids after the 135 huntingtin residues (encoded by exons 1 to 3). However, no such truncated protein is produced. PCR-WT and PCR-MUT denote PCR products from wild-type and mutant alleles. (B) Huntingtin expression in ES cell lines. Protein immunoblot of protein extracts from normal human lymphoblast cells (HL); mouse brain (MB); and wild-type R1 (+/+), heterozygote R1Hdh4/5-1 (+/-), and homozygous mutant R1Hdh4/5-1d1 (-/-) ES cells probed with HF1, a polyclonal antiserum to huntingtin (5). A 200-kD marker (arrowhead) is myosin and mouse and human huntingtin migrate at ~340 to 350 kD. Preincubation of HF1 with huntingtin fusion protein specifically eliminates the human (H) and mouse (M) huntingtin bands (5). Additional bands are nonspecific, as they were not affected by antigen preabsorption and were detected by preimmune serum. HP1 antiserum, directed at the extreme NH<sub>2</sub>-terminus of huntingtin, did not detect novel lower molecular weight bands in mutants in separate experiments where gels were run under conditions aimed to detect smaller proteins, particularly in the 15- to 20-kD range (5).

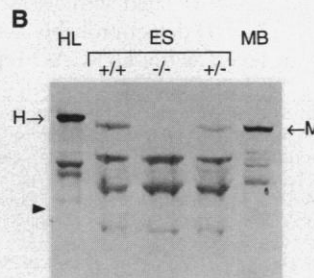


**Table 1.** Genotypes and phenotypes exhibited by progeny of *Hdh*<sup>+/-</sup> intercrosses. N, morphology within normal variation; A, characteristic abnormal mutant morphology.

Age	Litters	Genotypes and phenotypes					
		+/+		+/-		-/-	
		N	A	N	A	N	A
Newborn	25	76	0	160	0	0	0
E9.5	2	6	0	9	0	0	5*
E8.5	4	12	0	21	0	0	9*
E7.5	5	14	0	28	0	0	12†
E7.0	2	9	0	7	0	0	6‡
Total	38	117	0	225	0	0	32

\*Resorption sites and resorbing embryos. †Embryos with abnormal morphology. ‡Embryos small and thin.

ing of a primitive streak that was not fully extended. *HNF-3 $\beta$*  and *gsc* detected diffuse, disorganized patches of cells rather than discrete structures near the distal pole.

While this manuscript was in review, Nasir *et al.* (14) described a different mutation in *Hdh* in which exon 5 was targeted, yielding an allele that produces a truncated ~20-kD protein from exons 1 to 4 and a portion of exon 6. Mice heterozygous for this mutation were behaviorally distinguishable, displayed cognitive deficits, and had a reduced subthalamic nucleus. Homozygotes displayed embryonic lethality, but with a less severe phenotype than that reported here, including two phenotypically normal mutant homozygotes at E8.5. The differenc-

es in phenotype between the two types of *Hdh* mutation may prove revealing concerning the NH<sub>2</sub>-terminal region of huntingtin and augur the need for caution in interpreting attempts to model HD by transgenesis with a human expression construct.

Our studies demonstrate that homozygous mutant embryos with complete *Hdh* inactivation implant normally, develop a primitive streak and mesoderm, have abnormal cellular morphology, and degenerate rapidly between E7 and E8.5, with cell death first apparent in the embryonic ectoderm. This phenotype does not reflect a distinctive pattern of normal expression of *Hdh*, which is already on in ES cells (Fig. 1B), and is relatively uniformly expressed in the early embryo (13). Thus, huntingtin, although not essential in cultured ES cells, is required at the multicellular level for appropriate and complete development. The phenotype produced by huntingtin deficiency is unique. Indeed, few other gene knock-outs produce death at gastrulation, and these display significant differences (15). Inactivation of *HNF-4* and *HNF-3 $\beta$*  (transcription factors with restricted expression patterns) results in greater developmental heterogeneity of embryonic lethality (E6.5 to E10.5). A transgene insertion in *fug1*, a gene with ubiquitous expression, also produces rapid cell death between E6.5 and E8.5, but these embryos fail to elaborate any mesoderm. That complete *Hdh* inactivation produces a distinct phenotype suggests that huntingtin may provide a new window on early embryonic development, before the emergence at E8.0 to E8.5 of the neural tube, the precursor of the HD defect's target tissue in humans.

Among human trinucleotide repeat disorders (16), the mode of action of the defect is known only in Fragile X mental retardation, where *FMR1* expression is suppressed (17), permitting a useful model to be generated by inactivation of the mouse homolog (18). By contrast, complete inactivation of *Hdh* does not cause an HD-like phenotype, which favors a gain of function model for the

human disorder. The new property of huntingtin conferred by the expanded polyglutamine segment must be peculiarly detrimental to selected adult neurons but need not necessarily act via huntingtin's normal biochemical pathway. The gain of function hypothesis is also amenable to testing by manipulation of *Hdh*, with the expectation that introduction of an expanded polyglutamine segment into mouse huntingtin will generate an accurate mouse model of HD.

REFERENCES AND NOTES

1. J. B. Martin and J. F. Gusella, *N. Eng. J. Med.* **315**, 1267 (1986); S. E. Folstein, *Huntington's Disease. A Disorder of Families* (Johns Hopkins Univ. Press, Baltimore, MD, 1989).
2. J. P. Vonsattel *et al.*, *Neurol. Exp. Neuropath.* **44**, 559 (1985).
3. Huntington's Disease Collaborative Research Group, *Cell* **72**, 971 (1993). Reviewed in J. F. Gusella, M. E. MacDonald, C. M. Ambrose, M. P. Duyao, *Arch. Neurol.* **50**, 1157 (1993); J. F. Gusella and M. E. MacDonald, *Semin. Cell Biol.* **6**, 21 (1995).
4. Y. Trottier *et al.*, *Nat. Genet.* **10**, 104 (1995); Y. S. Jou and R. M. Myers, *Hum. Mol. Genet.* **4**, 465 (1995); A. H. Sharp *et al.*, *Neuron* **14**, 1065 (1995); M. DiFiglia *et al.*, *ibid.*, p. 1075.
5. F. Persichetti *et al.*, *Mol. Med.* **1**, 374 (1995).
6. C. M. Ambrose *et al.*, *Somat. Cell Mol. Genet.* **20**, 27 (1994).
7. G. T. Barnes *et al.*, *ibid.*, p. 87; B. Lin *et al.*, *Hum. Mol. Genet.* **3**, 85 (1994). Mouse huntingtin is 91% identical to human, with the most notable difference in the polyglutamine segment where normal humans have 13 to 36 glutamines encoded by the polymorphic segment (CAG)<sub>n</sub>(CAA)<sub>2</sub>, whereas the mouse has 7 consecutive glutamine residues encoded by (CAG)<sub>2</sub>CAA(CAG)<sub>4</sub>.
8. ES cell manipulation and screening of *Hdh* targeted clones was done as described previously [W. Wurst and A. L. Joyner, (19), pp. 31-62]. *Hdh* targeting vector [pPNT-Hdh4/5 (Fig. 1) with 1.85 kb (Xba I fragment) and 5.5 kb (Hind III fragment) of *Hdh* DNA flanking exons 4 and 5] in the positive-negative selection vector pPNT [V. L. J. Tybulewicz, C. E. Crawford, P. K. Jackson, R. T. Bronson, R. C. Mulligan, *Cell* **65**, 1153 (1991)] was linearized with Sal I and electroporated into R1 ES cells (A. Nagy, J. Rossant, R. Nagy, W. Abramow-Newerly, J. C. Roder, *Proc. Natl. Acad. Sci. U.S.A.* **90**, 8424 (1993). Approximately 300 G418- and gancyclovir-resistant ES cell transformants were screened by Southern (DNA) blot assay.
9. Genomic DNA from ES cells, mouse tail clips, and embryos digested with Eco RV and Southern blots were hybridized to an exon 6 probe [151 base pairs (bp) according to standard methods (6)]. The targeting event was confirmed in ES cell clones by Southern blot with Xba I, Hind III, Xho I, Eco RI, and Sac I restriction digests (exon 3, *neo* probe). Polymerase chain reaction (PCR) amplification was two separate reactions using primer 1 (5'-ACGTGAGCTGTC-CAGGTGAGCC-3') and primer 2 (5'-TATAGAGT-TCTACTGTAGCCTTG-3') or primer 1 and primer 3 (5'-TCGCCGCTCCCGATTTCGCAGCGCATCG-3') (30 cycles at 94°C for 1 min, at 58°C for 1 min, and at 72°C for 1 min). Products were analyzed directly on ethidium-stained agarose gels or by Southern blot with the use of oligonucleotide probes specific for mutant or wild-type alleles.
10. R. M. Mortensen, D. A. Conner, S. Chao, A. A. T. Geisterfer-Lowrance, J. G. Seidman, *Mol. Cell. Biol.* **12**, 2391 (1992).
11. ES cell lines (three targeting events) were aggregated with CD1 morulae to generate chimeric males [A. Nagy and J. Rossant, in (19), pp. 147-180], which were bred to CD1 and C57BL/6J females. F<sub>2</sub> animals were generated by intercrossing of F<sub>1</sub> offspring of chimeric males representing a single ES cell line. The morning the vaginal plug was observed was E0.5.

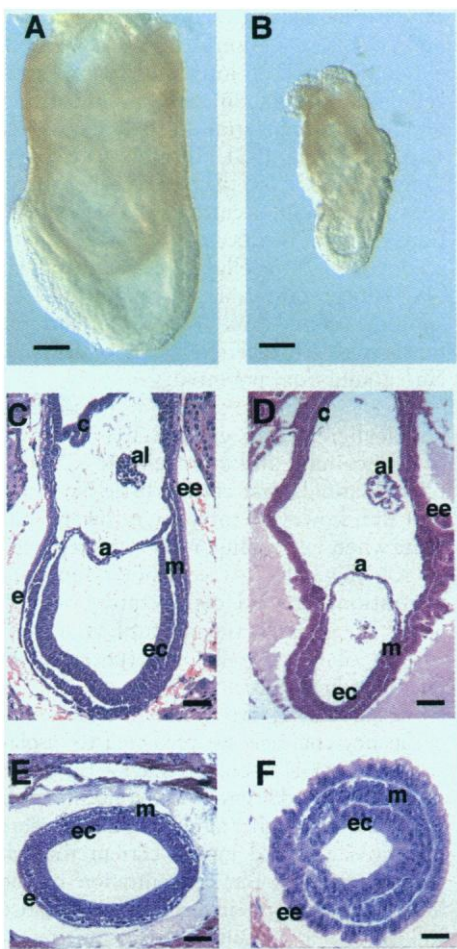


**Fig. 2.** Morphology and histology of E7.5 wild-type and homozygous mutant embryos. Examples of wild-type (A, C, and E) and homozygous mutant (B, D, and F) E7.5 embryos are shown as whole embryos (A) and (B) with the ectoplacental cone and parietal endoderm removed and as sagittal (C) and (D) and transverse (E) and (F) hematoxylin-eosin stained sections. (E) and (F) represent similar regions of the upper primitive streak (c, chorion; al, allantois; ee, extra-embryonic endoderm; a, amnion; e, embryonic endoderm; m, embryonic mesoderm; and ec, embryonic ectoderm). Scale bar: 100  $\mu$ M in (A) and (B); 50  $\mu$ M in (C) to (E); 25  $\mu$ M in (F).

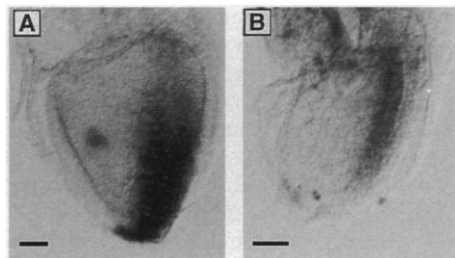


**Fig. 3.** Whole-mount analysis of *Brachyury* (*T*) RNA expression. Whole-mount RNA of normal (A) and *Hdh* homozygous mutant (B) embryos was analyzed for *Brachyury* (*T*) expression by RNA in situ hybridization (13). In 4/4 homozygous mutants, *T* expression is most apparent in the shortened primitive streak. Scale bar, 25  $\mu$ M.

12. Heterozygous mice that were observed up to 9 months of age did not show behavioral abnormalities during normal handling. Proteins from brains of 4-month-old heterozygotes and sex-matched littermates ( $n =$  two pairs) were analyzed by protein immunoblot with HF1 and HP1, polyclonal rabbit antisera to human huntingtin directed against epitopes near the COOH-terminus and the NH<sub>2</sub>-terminus, respectively (5). Neuropathological examination of 4-month-old heterozygotes and sex-matched CD1 littermates ( $n =$  four pairs) was carried out on hematoxylin-eosin stained 7- $\mu$ m serial sections of paraffin-embedded whole brain, including the brain stem (2). In sections of the cortex, cerebellum, and basal ganglia, the number of abnormal neurons (five fields) was counted, and no significant morphological alterations between wild-type and heterozygous animals were observed. Neuropathological examination of 4-month-old heterozygotes and sex-matched C57BL/6J littermates ( $n =$  two pairs) was carried out on similar serial sections, with adjacent sections being stained with hematoxylin-eosin, hematoxylin-eosin-Luxol fast blue, and cresyl violet (Nissl). Blinded examination by three neuropathologists detected no diagnostic abnormality in any region, including the basal ganglia (caudate putamen, globus pallidus, amygdala, substantia nigra reticulata and compacta, and subthalamic nucleus).
13. RNA in situ hybridization of dissected embryos was done as described in R. A. Conlon and B. G. Herrmann, *Methods Enzymol.* **225**, 373 (1993), with the use of the following probes: *Brachyury (T)* [B. G. Herrmann, *Development* **113**, 913 (1991)]; *gsc* [M.

- Blum *et al.*, *Cell* **69**, 1097 (1992)]; *HNF-3 $\beta$*  [A. P. Monaghan, A. P. Kessner, E. Grau, G. Schutz, *Development* **119**, 567 (1993)]; and *Hdh* (from a 1852-bp Pst I fragment representing bases 7819 to 9670 of mouse *Hdh* complementary DNA, GenBank no. L28827).
14. J. Nasir *et al.*, *Cell* **81**, 811 (1995).
15. A. J. Copp, *Trends Genet.* **11**, 87 (1995).
16. P. J. Willems, *Nat. Genet.* **8**, 213 (1994).
17. A. J. M. H. Verkerk *et al.*, *Cell* **65**, 905 (1991); M. Pieretti *et al.*, *ibid.* **66**, 817 (1991); J. S. Sutcliffe *et al.*, *Hum. Mol. Genet.* **1**, 397 (1992).
18. The Dutch-Belgium Fragile X Consortium, *Cell* **78**, 23 (1994).
19. *Gene Targeting: A Practical Approach*, A. L. Joyner, Ed. (Oxford Univ. Press, Oxford, 1993).
20. The authors thank E. Li and M. Kownacka for assistance in culturing ES cells; S. Chui for his expert help with the histology; E. P. Richardson for neuropathological consultation; J. Rossant for marker probes; and N. Rosenthal, C. Neville, and B. Morgan for valuable discussion. Supported by NIH grants NS32765 and NS16367 and by grants from Bristol-Myers Squibb Inc. (J.F.G. and A.J.), the Hereditary Disease Foundation, and the Huntington's Disease Society of America. S.M. and M.D. were supported by fellowships from the Huntington's Disease Society of America and the Hereditary Disease Foundation, respectively. During the course of the work, A.J. was a Medical Research Council of Canada Scientist and International Scholar of the Howard Hughes Medical Institute.

12 April 1995; accepted 22 June 1995

## Permeation Selectivity by Competition in a Delayed Rectifier Potassium Channel

Stephen J. Korn and Stephen R. Ikeda

Permeation selectivity was studied in two human potassium channels, Kv2.1 and Kv1.5, expressed in a mouse cell line. With normal concentrations of potassium and sodium, both channels were highly selective for potassium. On removal of potassium, Kv2.1 displayed a large sodium conductance that was inhibited by low concentrations of potassium. The channel showed a competition mechanism of selectivity similar to that of calcium channels. In contrast, Kv1.5 displayed a negligible sodium conductance on removal of potassium. The observation that structurally similar potassium channels show different abilities to conduct sodium provides a basis for understanding the structural determinants of potassium channel selectivity.

Delayed rectifier K<sup>+</sup> channels are exposed to large electrochemical gradients of both Na<sup>+</sup> and K<sup>+</sup>. Rapid repolarization of the action potential therefore requires that these channels be highly selective for K<sup>+</sup> over Na<sup>+</sup>. K<sup>+</sup> channels contain multiple ion binding sites within the pore that can be occupied simultaneously by more than one ion (1, 2). The observation that K<sup>+</sup> currents are partially blocked by Na<sup>+</sup> suggests that Na<sup>+</sup> can bind within the channel pore (3, 4). However, K<sup>+</sup> channels have almost universally been shown to be impermeable to Na<sup>+</sup> (3–5). The mechanism that

prevents the small Na<sup>+</sup> ion from conducting, while permitting several larger ions (for example, K<sup>+</sup>, Rb<sup>+</sup>, NH<sub>4</sub><sup>+</sup>, and Cs<sup>+</sup>) to conduct, has not been elucidated.

L-Type Ca<sup>2+</sup> channels represent another class of multi-ion channels that displays extremely high ion specificity. However, removal of Ca<sup>2+</sup> permits Na<sup>+</sup> to permeate, which has led to a model in which competition between Ca<sup>2+</sup> and Na<sup>+</sup> for intrapore binding sites determines which ion occupies the channel and conducts (6).

Recently, neuronal K<sup>+</sup> channels from rat superior cervical ganglia and chick dorsal root ganglia were shown to conduct Na<sup>+</sup> on removal of K<sup>+</sup> (7). The selectivity mechanism of these channels appeared similar to that of Ca<sup>2+</sup> channels. We now show that two structurally similar K<sup>+</sup> channels allow Na<sup>+</sup> to permeate in the absence of

K<sup>+</sup>. However, whereas Na<sup>+</sup> conductance through one channel (Kv2.1) was substantial, Na<sup>+</sup> conductance through the other (Kv1.5) was negligible.

Mouse L cells were injected with complementary RNA that encoded one of two human K<sup>+</sup> channels, Kv2.1 or Kv1.5 (8). One day after injection, membrane currents carried by K<sup>+</sup> or Na<sup>+</sup> through these channels were examined by the whole-cell patch clamp technique (9). In solutions that contained high external Na<sup>+</sup> and high internal K<sup>+</sup> concentrations (10), both channels displayed typical depolarization-evoked delayed rectifier K<sup>+</sup> currents (Figs. 1A and 2A). With K<sup>+</sup> and Na<sup>+</sup> equilibrium potentials set to  $-87$  and  $>+125$  mV, respectively, currents through Kv2.1 reversed at  $-80$  mV (Fig. 1B), indicating that they were carried almost exclusively by K<sup>+</sup>.

In cells containing Kv2.1 channels, elimination of both intracellular and extracellular K<sup>+</sup> resulted in large inward currents during both depolarization and repolarization steps (Fig. 1C). With *N*-methylglucamine (NMG<sup>+</sup>) in the pipette solution, no outward current occurred with depolarizations as high as  $+80$  mV (Fig. 1D). With symmetrical intracellular and extracellular Na<sup>+</sup> concentrations and asymmetrical Cl<sup>-</sup> concentrations (and no K<sup>+</sup>), currents through Kv2.1 reversed at the calculated Na<sup>+</sup> equilibrium potential.

Kv1.5 channels carried a measurable but negligible Na<sup>+</sup> current after removal of intracellular and extracellular K<sup>+</sup> (Fig. 2B). Channels that carried little Na<sup>+</sup> current did, however, carry large inward currents when extracellular Na<sup>+</sup> was replaced by K<sup>+</sup> (Fig. 2B). At equimolar ion concentrations, inward conductance of Na<sup>+</sup> was  $0.79 \pm 0.20\%$  (mean  $\pm$  SEM;  $n = 4$ ) of that of K<sup>+</sup> at  $-20$  mV (potential of peak conductance).

In mixtures of two permeant ions, multi-occupancy channels are predicted to display anomalous mole fraction behavior (2, 6). In this situation, addition of low concentrations of the ion with higher affinity for an intrapore binding site should inhibit current through the channel. As the concentration of the high-affinity ion is increased, conductance will increase as a result of electrostatic repulsion between multiple ions in the pore. Kv2.1 displayed anomalous mole fraction behavior in mixtures of Na<sup>+</sup> and K<sup>+</sup> (Fig. 3). In cells with 140 mM Na<sup>+</sup> outside and 140 mM NMG<sup>+</sup> inside, addition of low concentrations of extracellular K<sup>+</sup> resulted in a concentration-dependent decrease in inward Na<sup>+</sup> current (Fig. 3, A and C). The minimum current, measured at  $+20$  mV, occurred at  $\sim 3$  mM K<sup>+</sup> (11). Further increases in the extracellular K<sup>+</sup> concentration resulted in an increase in current magnitude. At a concentration of 140 mM of exclusively one ion, inward conduc-

S. J. Korn, Department of Physiology and Neurobiology, Box U-156, University of Connecticut, Storrs, CT 06269, USA. E-mail: korn@oracle.pnb.uconn.edu  
S. R. Ikeda, Department of Pharmacology and Toxicology, Medical College of Georgia, Augusta, GA 30912, USA.